7014–7024 *Nucleic Acids Research, 2023, Vol. 51, No. 13* *Published online 29 May 2023*
https://doi.org/10.1093/nar/gkad447

Protein oxidation increases SAMHD1 binding ssDNA via its regulatory site

Theresa L. Simermeyer, Stephanie Batalis, LeAnn C. Rogers, Owen J. Zalesak and Thomas Hollis*

Department of Biochemistry, Wake Forest School of Medicine, Winston-Salem, NC, USA

Received June 22, 2022; Revised April 21, 2023; Editorial Decision May 07, 2023; Accepted May 15, 2023

ABSTRACT

SAMHD1 dNTP hydrolase activity places it at the crossroad of several important biological pathways, such as viral restriction, cell cycle regulation, and innate immunity. Recently, a dNTPase independent function for SAMHD1 in homologous recombination (HR) of DNA double-strand breaks has been identified. SAMHD1 function and activity is regulated by several post-translational modifications, including protein oxidation. Here, we showed that oxidation of SAMHD1 increases ssDNA binding affinity and occurs in a cell cycle-dependent manner during S phase consistent with a role in HR. We determined the structure of oxidized SAMHD1 in complex with ssDNA. The enzyme binds ssDNA at the regulatory sites at the dimer interface. We propose a mechanism that oxidation of SAMHD1 acts as a functional switch to toggle between dNTPase activity and DNA binding.

GRAPHICAL ABSTRACT

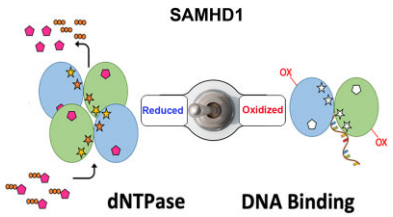

INTRODUCTION

SAMHD1 is a deoxynucleoside triphosphate (dNTP) hydrolase that catalyzes the hydrolysis of dNTPs into the constituent nucleoside and inorganic tripolyphosphate (1,2). SAMHD1 is an essential component of several critical biological functions that depend on dNTP regulation, such as DNA replication and repair, cell cycle progression, restriction of retroviral infections, and is a regulator of innate immune response (3). Catalytic activity of the enzyme is dependent on the formation of a homotetramer, which is induced by sequential binding of nucleotides to regulatory sites RS1 and RS2 (4–8). The RS1 pocket is specific for guanosine triphosphates (dGTP/GTP) while RS2 can then be occupied by any of the four dNTPs. SAMHD1 catalytic activity is also regulated by post-translational modifications including protein oxidation (9–11). Oxidation of SAMHD1 occurs through a redox switch composed of three cysteines, C341, C350 and C522 that inhibits catalytic activity by preventing tetramerization of the enzyme (9,10). Residue C522 serves as the initial sensor of H_2O_2 and mutation of C522 prevents protein oxidation and maintains a catalytically active enzyme in the presence of H_2O_2 (9,10). The oxidized C522 sulfenic acid undergoes a disulfide switching mechanism with C341 and C350 that results in a final C341–C350 disulfide bond in the inhibited form of SAMHD1 (9,12).

Recent data have revealed roles for SAMHD1 in DNA replication, repair, telomere stability, and regulation of innate immunity (13–20). Intriguingly, SAMHD1 can influence DNA repair independently of its dNTPase function by binding to damaged DNA and activating downstream effectors. SAMHD1 promotes degradation of nascent DNA at stalled replication forks through the stimulation of MRE11 exonuclease activity and activation of the ATR and CHK1 checkpoint (19). Additionally, SAMHD1 promotes DNA end resection and DNA double-strand break (DSB) repair through homologous recombination (HR) (15). SAMHD1 has been shown to colocalize with 53BP1 at DSBs and to recruit CtIP, and cells with reduced SAMHD1 expression are sensitive to DSB-inducing agents (13,15). In contrast, the SAMHD1 dNTPase function regulates DNA repair by non-homologous end joining (NHEJ) where low intracellular dNTP levels lead to shorter repair joints and reduce the insertion of distant DNA regions prior to end repair (21,22).

SAMHD1 has previously been shown to bind preferentially to single-stranded DNA (ssDNA) (23–27). Here, we show that oxidation of SAMHD1 increases its binding affinity for ssDNA. A crystal structure of oxidized SAMHD1 in complex with ssDNA shows that the enzyme binds ssDNA as a dimer, and that binding occurs at the reg-

*To whom correspondence should be addressed. Tel: +1 336 716 0768; Email: thollis@wakehealth.edu

© The Author(s) 2023. Published by Oxford University Press on behalf of Nucleic Acids Research.
This is an Open Access article distributed under the terms of the Creative Commons Attribution-NonCommercial License (http://creativecommons.org/licenses/by-nc/4.0/), which permits non-commercial re-use, distribution, and reproduction in any medium, provided the original work is properly cited. For commercial re-use, please contact journals.permissions@oup.com

ulatory sites. We also demonstrate that SAMHD1 oxidation occurs in a cell cycle-dependent manner, during S and G_2/M phases when HR and replication fork repair are active. Thus, we propose a mechanism in which oxidation redirects SAMHD1 function from dNTPase activity to DNA binding.

MATERIALS AND METHODS

Reagents and antibodies

Cell culture medium RPMI 1640 and DMEM:F12 were from Gibco. Primary antibodies for western blots were obtained from Sigma for SAMHD1 (HPA047072), Cell Signaling for Cyclin E1 (4129S) and Cyclin A2 (4656S), Abcam for Histone H3 phosphoS10 (ab14955), and EMD Millipore for GAPDH (CB1001). Secondary HRP-conjugated antibodies against rabbit (7074S) and mouse (7076S) were from Cell Signaling Technology. Nitrocellulose membranes were from Bio-Rad and Super Signal chemiluminescence reagent was from Thermo Scientific. DCP-Bio1 was from Xoder.

Expression and purification of SAMHD1 variants

The previously described pLM303-hSAMHD1 vector containing an N-terminal MBP-tag and an intervening rhinovirus 3C protease cleavage site was used to express full-length human SAMHD1 (aa 1–626) (9,28). All mutations to hSAMHD1 (C522A, 113–626aa and 113–626aa R451E) were synthesized and sequenced by GenScript using the pLM303-hSAMHD1 vector as a template. Expression vectors were transformed into *Escherichia* coli BL21* cells grown in LB medium under kanamycin selection until an $OD_{600} = 0.6$ was reached. Protein expression was induced by adding IPTG to a final concentration of 1 mM. Purification of all hSAMHD1 constructs was performed using amylose resin, Heparin HiTrap, and Superdex S200 size exclusion chromatography as described previously (9). The protein was concentrated, flash frozen in individual aliquots, and stored at −80°C until use.

DNA binding measurements

Binding affinities of SAMHD1 variants were measured using fluorescence anisotropy. Experiments were conducted using 5′-6-carboxy-fluoroscein (6-FAM) labeled DNA oligo constructs detailed in the Table 1 below and obtained from Integrated DNA Technologies (IDT). SAMHD1 protein was passed through a microspin column packed with BioGel-P6 (BioRad) equilibrated with binding buffer (40 mM Tris pH 7.5, 100 mM NaCl, 5 mM $MgCl_2$, 0.5% glycerol, 0.1 mM EDTA and 100 μg/ml BSA) to remove all reducing reagents from the protein. In experiments where SAMHD1 was kept under reducing conditions 10 mM DTT and 2 mM TCEP were kept in the reaction solution. Oxidation of SAMHD1 was performed by incubating 150 μM protein with 300 μM H_2O_2 for 20 min. The remaining H_2O_2 was then removed by passing protein through a microspin column packed with BioGel-P6 (Bio-Rad). When used, nucleotides (GTP/dATP) were added to the protein after treatment with oxidizing agents but prior to incubation with the 6-FAM labeled oligonucleotide. In all anisotropy experiments, increasing concentrations of SAMHD1 were incubated with 5 nM of DNA in the presence of binding buffer. Anisotropy measurements were recorded at 25°C on an Infinite M100 Pro microplate reader with a fluorescence polarization module (Tecan Group, Ltd), using an excitation wavelength of 470 nm and an emission wavelength of 530 nm.

Anisotropy data were normalized using the equation:

$$A = (A_{obs} - A_0)/A_{max}$$

Anisotropy values were plotted as a function of protein concentration and fit to either hyperbolic or sigmoidal binding curves using the program Prism (GraphPad). Each anisotropy curve plotted is the average of at least 3 independent experiments with the error bars on the graphs representing the standard deviation. SAMHD1 enzyme used in the anisotropy experiments was tested to ensure it does not have nuclease activity (Supplementary Figure S1).

SAMHD1 structure determination

SAMHD1-DNA complexes were crystallized by the sitting drop vapor diffusion technique. Protein was exchanged into buffer containing 20 mM Tris pH 7.5 and 300 mM NaCl by spinning through a column packed with BioGel-P6 (Bio-Rad) equilibrated with the buffer. Prior to crystallization, the DNA complex was formed by diluting protein to 5 mg/ml in gel filtration buffer and incubating with 220 μM DNA (Integrated DNA Technologies) and 1 mM $MgCl_2$. We previously showed SAMHD1 is prone to oxidation in solution in the absence of any reducing reagent (9). Crystals were prepared by sitting drop vapor diffusion method. One μl each of proteinDNA complex and reservoir solution was added to a CrystalEX microplate (Corning) containing 100 μl of reservoir solution. Reservoir solution contained 100 mM Tris–HCl pH 7.5, 200 mM $CaCl_2$, 20% PEG 3350 and 4% 2-methyl-2,4-pentanediol (MPD) for cryo-preservation. Crystals grew at room temperature within one week. Crystals were mounted on a nylon loop and flash-frozen in liquid nitrogen.

Diffraction data were collected at the Stanford Synchrotron Radiation laboratory (SSRL) on beamline 12–2 using a Pilatus 6M detector and processed and integrated using HKL3000. The data statistics are summarized in Table 1. Structures were solved by maximum likelihood molecular replacement with the SAMHD1 dimer (PDB ID: 3u1n (2)) as the search model using the program PHASER and model building was done with Coot (29). The model was refined in PHENIX (version 1.18.2_3874) (30) with iterative rounds of phenix.refine and clashes and stereochemical parameters were identified using MolProbity (31). TM-scores were generated using the TM-score online server (https://zhanglab.ccmb.med.umich.edu/TM-score/) (32). The program, Pymol version 2.3.3 (Schrodinger), was used to make structural figures.

Cell culture

PC3, prostate cancer epithelial cells from ATCC stocks, were grown, maintained, and treated at 37°C with 5% CO_2

Table 1. DNA oligos used for DNA binding

Oligo name	Sequence
ssDNA 30 mer	3′ GAT GGA CAG ACC AGG ACA GAG TTG TGA CAG 5′ - FAM
dsDNA 30 mer	5′ CTA CCT GTC TGG TCC TGT CTC AAC ACT GTC 3′ 3′ GAT GGA CAG ACC AGG ACA GAG TTG TGA CAG 5′ - FAM
ssDNA 57mer	3′ TTC GCC ACG ATC TCG ACA GAT GCT GGT TAA CTC GCC GGA GCC GTG GCC CTA AGA GGT 5′ - FAM
3′ Overhang	5′ T GAG CGG CCT CGG CAC CGG GAT TCT CCA 3′ 3′ TTC GCC ACG ATC TCG ACA GAT GCT GGT TAA CTC GCC GGA GCC GTG GCC CTA AGA GGT 5′ - FAM
5′ Overhang	5′ AAG CGG TGC TAG AGC TGT CTA CGA CCA AT 3′ 3′ TTC GCC ACG ATC TCG ACA GAT GCT GGT TAA CTC GCC GGA GCC GTG GCC CTA AGA GGT 5′ - FAM
3′ Fork	5′ AATTG T GAG CGG CCT CGG CAC CGG GAT TCT CCA 3′ 3′ TTC GCC ACG ATC TCG ACA GAT GCT GGT TAA CTC GCC GGA GCC GTG GCC CTA AGA GGT 5′ - FAM
5′ Fork	CTGAA 3′ 5′ AAG CGG TGC TAG AGC TGT CTA CGA CCA AT 3′ TTC GCC ACG ATC TCG ACA GAT GCT GGT TAA CTC GCC GGA GCC GTG GCC CTA AGA GGT 5′ - FAM

in RPMI 1640 medium supplemented with 10% fetal bovine serum, L-glutamine, penicillin, and streptomycin.

Cell cycle synchronization and harvest

PC3 cells (~3×10^5) were grown in 100 mm dishes synchronized at the G_2 to M transition 48 h post seeding using successive blocks in thymidine and nocodazole. Cells were blocked in 2 mM thymidine supplemented culture media for 24 h then released into unsupplemented media for 2 h. After the 2 h release cells were blocked in 100 ng/ml nocodazole supplemented culture media for 9 h then released into unsupplemented culture media. Cells were harvested for Western blot analysis of SAMHD1 oxidation and cell cycle markers at time of release from nocodazole block and at 2, 6, 14, 16, 18, 20 and 22 h post release from nocodazole. For each experiment, an asynchronous plate of cells was harvested as a control.

DCP-bio1 labeling and pulldown of oxidized proteins

For all cell cycle synchronization experiments oxidation of SAMHD1 was measured using the dimedone-based reagent for labeling cysteine-sulfenic acids, DCP-Bio1 (9,33,34). Cells were grown in 100 mm dishes and blocked at the G_2 to M transition as described above and after release of chemical block DCP-Bio1 was added with lysis buffer to chemically trap sulfenic acid proteins. Lysis buffer (50 mM Tris–HCl, 100 mM NaCl, 2 mM EDTA, 0.1% SDS, 0.5% sodium deoxycholate, 1 mM phenylmethylsulphonyl fluoride (PMSF), 10 μg/ml aprotinin, 10 μg/ml leupeptin, 50 mM NaF, and 1 mM sodium vanadate) was freshly prepared and supplemented with 1 mM DCP-Bio1, 10 mM NEM, 10 mM iodoacetamide and 200 U/ml catalase. Lysis buffer (100 μl/plate) was added to each plate, then cells were scraped from plates, transferred to Eppendorf tubes, incubated on ice for 30 min, and frozen at −80°C. For affinity capture and elution of labeled proteins, unreacted DCP-Bio1 was removed immediately following thawing cells using a P6 BioGel spin column. Samples were then assayed for protein concentration, diluted to 1.0 mg/ml protein into 400 μl buffer containing a final concentration of 2 mM urea. Samples were precleared with Sepharose CL-4B beads (Sigma), applied to columns containing high-capacity streptavidin-agarose beads from Pierce, and then incubated overnight at 4°C. Multiple washes of the beads were performed (at least four column volumes and two washes each) using, in series, 1% SDS, 1 M NaCl, 10 mM DTT, 50 mM ammonium bicarbonate and water before elution in Laemmli sample buffer. Samples were stored at −80°C as needed and analyzed by Western Blot as described below.

Western blotting

Chemically synchronized cells were harvested in lysis buffer supplemented with DCP-Bio1, NEM, iodoacetamide, and catalase. All samples were harvested, frozen, cleared of excess DCP-Bio1, and assayed for protein concentration as described above. Lysate samples (typically 20 μg protein/lane) and pull-down samples (typically 40 μg protein/lane) were resolved on SDS polyacrylamide gels, then transferred to nitrocellulose membranes, probed with protein-specific antibodies, and visualized using Super Signal chemiluminescence reagent.

RESULTS

SAMHD1 oxidation increases DNA binding affinity

Because cysteine oxidation at C341/C350/C522 inhibits the SAMHD1 dNTPase function, we hypothesize this is a mechanistic switch to downregulate dTNPase function and upregulate DNA binding. We measured the effect of SAMHD1 protein oxidation on DNA binding affinity by fluorescence anisotropy using fluorescein-labeled DNA oligonucleotides (Figure 1). The binding affinity of oxidized SAMHD1 for ssDNA is 40-fold higher compared to reduced protein, with K_d values of 0.8 ± 0.3 μM and 33 ± 8 μM respectively (Figure 1). SAMHD1 has a lower affinity for dsDNA ($K_d = 49 \pm 17$ μM) and oxidation of SAMHD1 has little effect on dsDNA binding (Figure 1). These results agree with previous data showing that SAMHD1 preferentially binds to ssDNA (24), and suggests that oxidation enhances DNA binding function of SAMHD1.

To confirm that oxidation of SAMHD1 through the redox switch residues contributes to increased binding affinity, we mutated the redox-sensing cysteine 522 to an alanine (C522A) to prevent protein oxidation (9). Oxidation did not increase the binding affinity of SAMHD1 C522A for ssDNA with K_d values of 7.8 ± 3.0 μM (oxidized) and 8.9 ± 3.7 μM (reduced) (Figure 1). Additionally, the SAMHD1

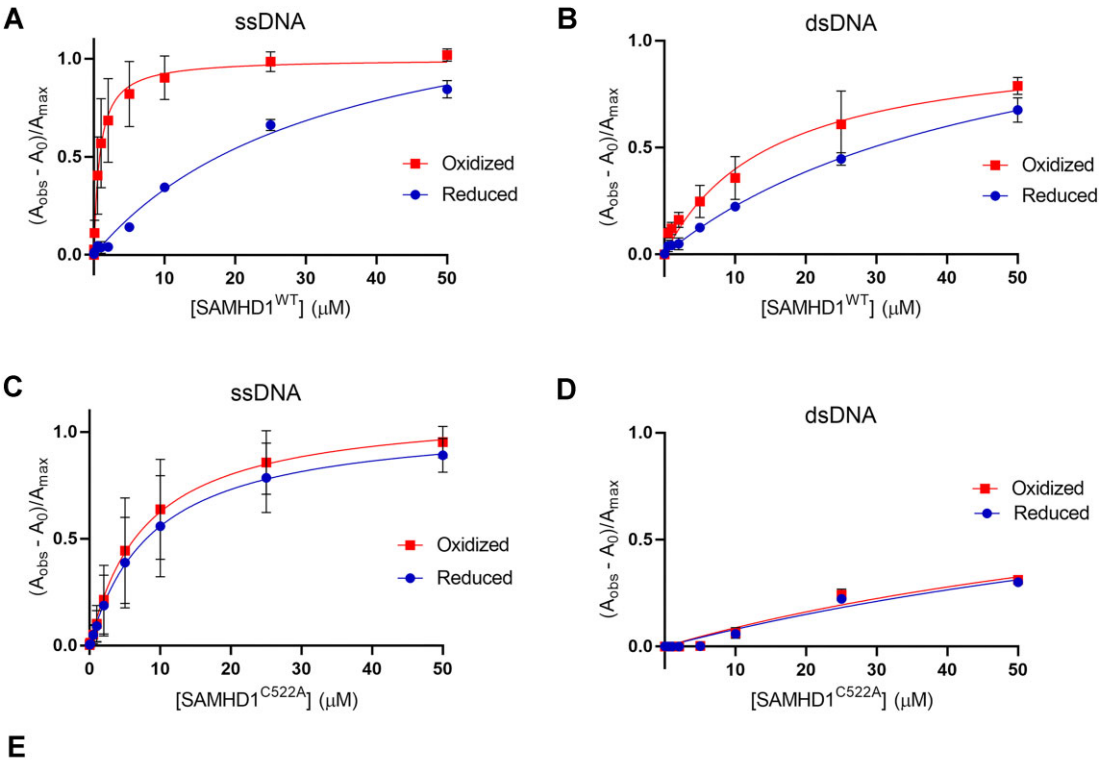

E

DNA	SAMHD1^{WT}	K_d(μM)	SAMHD1^{C522A}	K_d(μM)
ssDNA	Reduced	33 ± 8 μM	Reduced	8.9 ± 3.7 μM
ssDNA	Oxidized	0.8 ± 0.3 μM	Oxidized	7.8 ± 3 μM
dsDNA	Reduced	49 ± 17 μM	Reduced	Undetermined
dsDNA	Oxidized	15 ± 9 μM	Oxidized	Undetermined

Figure 1. Oxidation of SAMHD1 facilitates ssDNA but not dsDNA binding. (**A**) Binding of SAMHD1 WT to ssDNA 30mer under oxidizing (red) and reducing (blue) conditions, as measured by fluorescence anisotropy. (**B**) Binding of SAMHD1 WT to dsDNA 30mer. (**C**) Binding of oxidation insensitive SAMHD1 C522A to ssDNA 30mer. (**D**) Binding of oxidation insensitive SAMHD1 C522A to dsDNA 30mer. (**E**) Calculated binding affinities ±95% confidence interval for SAMHD1 WT and C522A for ssDNA and dsDNA under oxidizing and reducing conditions. Graphs show normalized anisotropy values as a function of protein concentration. All error bars represent the standard deviation. Dissociation constants (K_d) were calculated by fitting the data to the equation for one site specific binding.

C522A mutant had no measurable affinity for dsDNA (Figure 1). It has been previously reported that SAMHD1 phosphorylation promotes DNA repair activity (19). We measured the ssDNA binding affinity of the SAMHD1 T592E phosphomimetic under oxidizing and reducing conditions to determine if there might be a synergistic effect between oxidation and phosphorylation on the DNA binding affinity. However, the data show (Supplementary Figure S2) that the T592E SAMHD1 has similar K_d values as the wild-type protein under both oxidizing and reducing conditions. Together these data indicate that oxidation of the redox switch, which inhibits dNTPase activity, increases ssDNA binding affinity.

Given that SAMHD1 has been implicated in double-strand break repair (15,19,21,22) we investigated the impact of oxidation on SAMHD1 binding to DNA structures that mimic those found at DSB sites. We measured DNA binding affinity of oxidized and reduced SAMHD1 for four different duplex DNA structures containing single-stranded overhangs using fluorescence anisotropy. Two of the structures were formed by annealing a DNA 28-mer and 56-mer to form a construct with 28 bases of dsDNA and 28 bases of ssDNA as either a 5′ overhang or 3′ overhang. We also created a second set of DNA constructs that mimic DNA replication forks by adding five additional non-complementary bases at the dsDNA-ssDNA junction of the previous constructs (Figure 2).

Intriguingly, two distinct modes of binding were observed based on the polarity of the ssDNA overhang. When the overhang or fork was on the DNA 5′ end, the binding data fit a hyperbolic curve similar to the binding data of SAMHD1 with ssDNA (Figure 2A). As with binding to ssDNA, oxidation of SAMHD1 increased the binding affinity for each construct by approximately 5-fold (Figure 2A and C). However, when the overhang or fork was on the 3′ end, the binding data fit to a distinctly sigmoidal curve indicative of cooperative binding (Figure 2B and C). Oxidation of SAMHD1 increases the positive cooperativity of the interaction as measured by the Hill slope of the curve, from 2.3 to 4.3 for the 3′ overhang and 1.9 to 3.1 for the 3′ fork DNA (Figure 2E). These data indicate that oxidation of SAMHD1 enhances the binding affinity to a variety of

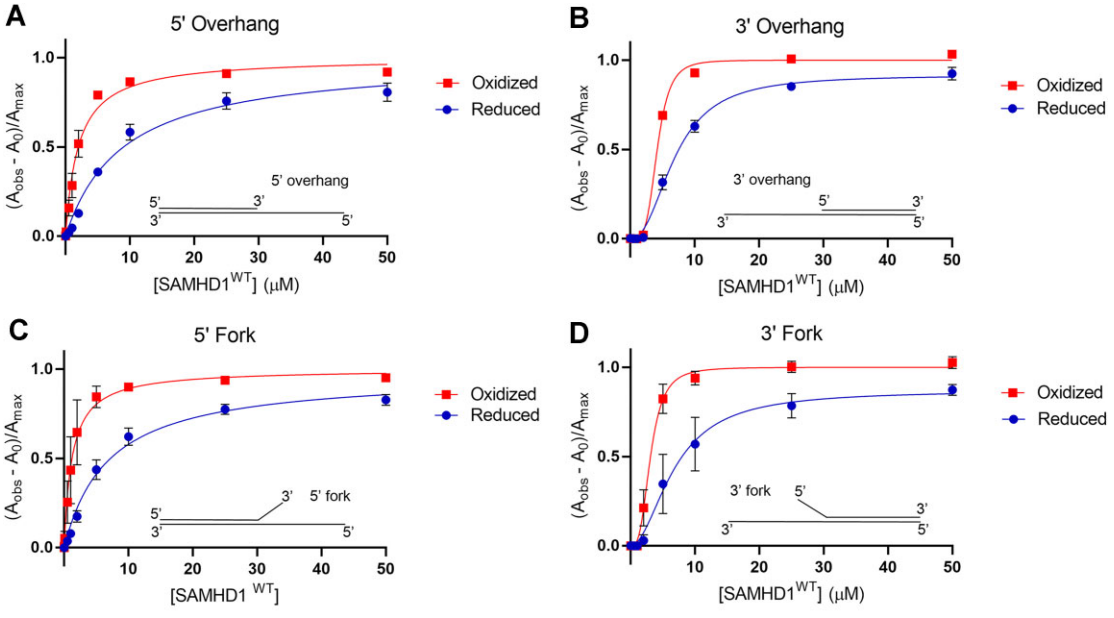

E

DNA	SAMHD1	K_d (μM)	Hill Coefficient
5' overhang	Reduced	9.0 ± 1.9 μM	N/A
5' overhang	Oxidized	2.0 ± 0.3 μM	N/A
3' overhang	Reduced	6.7 ± 0.4 μM	2.3 ± 0.2
3' overhang	Oxidized	4.1 ± 0.1 μM	4.3 ± 0.7
5' fork	Reduced	6.8 ± 1.2 μM	N/A
5' fork	Oxidized	1.2 ± 0.3 μM	N/A
3' fork	Reduced	6.6 ± 1.2 μM	1.9 ± 0.7
3' fork	Oxidized	3.0 ± 0.2 μM	3.1 ± 0.5

Figure 2. Oxidation of SAMHD1 enhances binding to complex DNA structures. (**A**) Binding of SAMHD1 WT to 5′ overhang DNA under oxidizing (red) and reducing (blue) conditions, as measured by fluorescence anisotropy. (**B**) Binding of SAMHD1 WT to 3′ overhang DNA. (**C**) Binding of SAMHD1 WT to 5′ fork DNA. (**D**) Binding of SAMHD1 WT to 3′ fork DNA. (**E**) Calculated binding affinities and Hill coefficients ±95% confidence interval for SAMHD1 WT with overhang and fork constructs. Graphs represent normalized anisotropy values relative to protein concentration. All error bars represent the standard deviation. Dissociation constants (K_d) were calculated by fitting the data to the equation for one site specific binding. Hill coefficients were calculated by fitting the data to the equation for specific binding with Hill slope.

DNA constructs, including ssDNA and mixed ss/dsDNA structures found at DSBs, and that SAMHD1 interacts with the DNA in a structure-dependent fashion.

SAMHD1 binds ssDNA at the nucleotide regulatory sites

The structure of the oxidized SAMHD1 catalytic domain was determined in complex with ssDNA and reveals the protein binds to DNA as a dimer (Figure 3 and Supplementary Table S1). The protein was crystallized with a 5mer ssDNA (CATGT), but only the three nucleotides on the 3′ terminus (TGT) have electron density in the structure. Interestingly, the ssDNA occupies the two nucleotide regulatory sites with the dG nucleotide occupying the guanine regulatory site, known as RS1, and the 3′ dT bound in the second site, known as RS2 (Figure 3). An examination of the complex shows SAMHD1 interacts with the DNA through several hydrogen bonds and cation-pi interactions, including residue R451 at RS1, similar to the structure of SAMHD1 in complex with regulatory nucleotides (6,8,35). The structure also shows a disulfide bond between residues C341 and C350 in all four monomers in the asymmetric unit (Figure 3), confirming SAMHD1 oxidation. A second structure of SAMHD1 in complex with ssDNA (CATTG) was also determined in which the guanine nucleotide was shifted to the terminal 3′ position (Supplementary Figure S3). This structure only has electron density for the two nucleotides on the 3′ terminus (TG). In this structure, the 3′ dG is also bound in the RS1 site and the RS2 site is unoccupied (Supplementary Figure S3). Additionally, the electron density is only able to confirm a single C341-350 disulfide bond in the dimer. The position of DNA in these two structures is similar to the previously observed position of phosphorothioate containing DNA binding to SAMHD1 (27), and consistent with the binding of DNA to dimer (not tetramer) seen by atomic force microscopy (24).

There are two dimer complexes in the asymmetric units of each structure of the SAMHD1–ssDNA complex, similar in arrangement to the previous structure of apo enzyme, which is catalytically inactive (2). Additionally, the active site contains electron density suggesting a single iron atom, similar to what has been seen previously (36), along

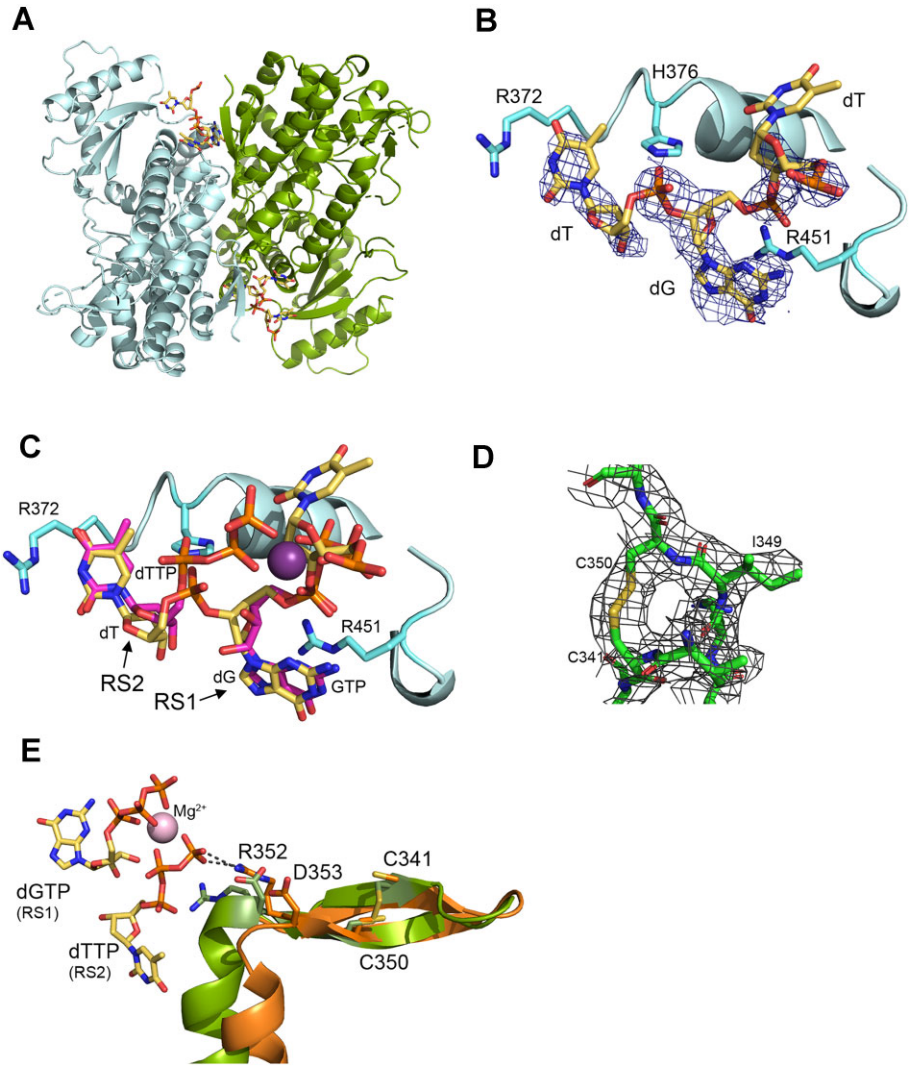

Figure 3. SAMHD1 binds ssDNA at regulatory sites. (**A**) Structure of SAMHD1 dimer with ssDNA bound at the dimer interface. One monomer in blue and the other in green with the ssDNA as a stick model. (**B**) Residues that interact with the ssDNA include R451 which forms cation-pi stacking interactions with the dG base (2Fo – Fc, electron density at 1σ). (**C**) Superposition of regulatory nucleotides from SAMHD1 tetramer structure (PDB ID: 4TNQ) shows that 2 nucleotides from the ssDNA bind in RS1 and RS2. (**D**) C341 and C350 form a disulfide bond in the structure as shown by 2Fo – Fc electron density (1σ) of the refined model. (**E**) A superposition of oxidized SAMHD1 (green) on the reduced enzyme with bound regulatory nucleotides (PDB ID: 4TNQ) reveals the C341–C350 disulfide produces a conformational change that shifts R352 and D353. Residue R352 is displaced by D353 to disrupt the interaction with the γ-phosphate of the deoxynucleotide in the RS2 site.

with a calcium ion are bound (Supplementary Figure S4). A superposition of the dimers from the two ssDNA complexes shows they are highly structurally similar to each other (rmsd 0.58 Å and TM-score 0.99) and to the dimer in the apo structure (rmsd 0.93 Å and TM-score 0.97) (32). The apo enzyme lacks the bound deoxynucleoside triphosphates in the RS1 and RS2 sites that induce tetramer formation of SAMHD1 necessary for catalytic activity (4,6,35). Although the ssDNA nucleotides occupy both the RS1 and RS2 in the structure bound to ssDNA (CATGT), they lack the necessary interactions with the third protomer at the regulatory sites to form a tetramer. Specifically, in structures of the SAMHD1 tetramer with the regulatory sites filled with nucleotides, residues R352, K354, and K523 from a third protomer interact with each of the phosphates of the nucleotide bound in the RS2 position and contribute to tetramer formation (Figure 3). Since there are no β and γ phosphates in the DNA oligonucleotide, these interactions are absent when SAMHD1 is bound to DNA. The formation of a dimer in response to oxidation, however, is consistent with our previous work showing that oxidation promotes the dimer and inhibits tetramer formation (9). We can see a mechanistic explanation of this in the oxidized dimers. The formation of a disulfide bond between C341 and C350 in the oxidized protein induces a conformational shift in the adjacent helix containing residue R352 (Figure 3). This movement results in the R352 side chain moving about 6 Å away and residue D534 moving to occupy its position. The negative charge on the D534 carboxylate is positioned to repel the γ phosphate of the regulatory nucleotide in RS2.

To confirm the guanine-specific interactions of the ssDNA at the RS1 site, DNA binding affinity of oxidized

SAMHD1 was measured in the presence of increasing concentrations of GTP to compete for the RS1 site and plotted as a fraction of maximal binding (Figure 4). These data show that GTP significantly decreases the binding affinity for ssDNA, indicating that GTP competes with ssDNA for RS1. At the highest concentration of GTP (0.5 mM) the fraction of maximal DNA binding is approximately 10%. In contrast, titration of dATP, which competes with ssDNA for the RS2 site, only reduced the fraction of maximal binding to approximately 60%. Additionally, the structures reveal that amino acid R451 directly interacts with the guanine base in the DNA oligo occupying the RS1 site (Figure 3). The R451E mutation shows no measurable DNA binding (Figure 4). Consistent with these data others have shown that the presence of GTP or dGTPαS, but not dATP, reduces SAMHD1 crosslinking to DNA (23).

Finally, since the structures were determined with the SAMHD1 catalytic HD domain (amino acids 113–626), we wanted to confirm that binding of ssDNA was not impacted by loss of the SAM domain. We compared the binding affinity for ssDNA of the HD domain to the full-length protein (Figure 4B). In line with previous reports, removing the SAM domain did not significantly affect the binding affinity for ssDNA (24). The HD domain has a $K_d = 0.5 \pm 0.1$ μM compared to full-length SAMHD1 with a $K_d = 0.8 \pm 0.3$ μM. Together, these data strongly support the binding of ssDNA in the nucleotide regulatory sites at the SAMHD1 dimer interface.

SAMHD1 is oxidized in a cell cycle-dependent manner.

Since oxidation of SAMHD1 enhanced ssDNA binding, we next looked for evidence of SAMHD1 oxidation during specific phases of the cell cycle when HR and replication fork repair are active (37–40). Oxidation of SAMHD1 was measured in PC3 cells synchronized using thymidine and nocodazole and released (41,42). We previously showed that SAMHD1 is oxidized in response to growth factor stimulation in several cell lines, including PC3 (9,11). To minimize the possible effects of nucleotide pool disruption or aberrant oxidation by the thymidine/nocodazole treatment, oxidation of SAMHD1 was examined over the 22 hours following cell cycle release by removal of the compounds. Oxidized proteins were labeled at the time of harvest with a dimedone-based probe conjugated to biotin (DCP-Bio1) and affinity captured using streptavidin beads (9,33,34). The labeled proteins and the corresponding total lysate were immunoblotted and probed with an anti-SAMHD1 antibody (Figure 5A and Supplementary Figure S5). The total lysate was also blotted and probed for the cell cycle markers cyclin E, cyclin A, and phospho-histone H3. Following synchronization, there is a pattern of SAMHD1 oxidation during the cell cycle in two distinct waves (Figure 5). The first is when cyclin E is high, indicative of S phase, and the second when phospho-histone H3 is high, indicative of the G_2 to M transition. The high level of SAMHD1 oxidation seen at release is likely an artifact of the thymidine/nocodazole treatment and therefore not included in the analysis. Based on these findings we conclude that SAMHD1 is oxidized in a cell cycle-dependent manner, with oxidation of SAMHD1 corresponding to S and G_2/M phases in which HR is functioning for the repair of stalled replication forks and DSB repair.

DISCUSSION

We and others have previously found that oxidation of SAMHD1 inhibits the triphosphohydrolase activity by preventing formation of the enzyme tetramer (9,10). Here we report that oxidation of SAMHD1 enhances binding affinity for ssDNA and determine the structure of oxidized SAMHD1 in complex with ssDNA. These data show that oxidized SAMHD1 has an increased affinity for ssDNA and duplex structures containing single-stranded overhangs. Consistent with others' findings, we observed that SAMHD1 has a higher affinity for ssDNA compared to dsDNA (23,24). Interestingly, Seamon *et al.* (24) showed that SAMHD1 ssDNA binding affinity increased with DNA length up to about 60 nt. While the current structures show only the nucleotides within the regulatory site, this suggests that ssDNA outside of the regulatory site also likely interacts with the SAMHD1 surface to provide additional binding affinity, and is also consistent with what has been observed previously by DNA-crosslinking and mass spectrometry analysis (23). The SAMHD1 C522A variant is resistant to protein oxidation (9) and did not increase DNA binding affinity after exposure to H_2O_2, with no measurable affinity for dsDNA. The C522A protein did show a slightly higher affinity for ssDNA than the reduced WT SAMHD1. This could potentially be explained by the fact that residue C522 is near the regulatory sites, and the mutation to alanine might lead to a local structural change that mildly enhances DNA binding but not to the same extent as formation of the C341/C350 disulfide. Given the opposing effects of oxidation on dNTPase activity and DNA binding, we propose that oxidation of SAMHD1 serves as a mechanism to shift protein function from dNTP catalysis to DNA binding (Figure 6).

The structure of the SAMHD1-ssDNA(CATGT) complex reveals that ssDNA binds to SAMHD1 at the dimer interface with a dG nucleotide in the sequence occupying the RS1 site and the 3′ dT nucleotide occupying the RS2 site. Examination of the structures reveals that the dG and dT nucleotides make several of the same interactions with SAMHD1 in the RS1 and RS2 sites as what is observed in nucleotide-bound structures. Altering the sequence of the ssDNA from CATGT to CATTG in the structure shows the DNA shifts to maintain the dG nucleotide in the RS1 site, suggesting that dG is the primary recognition element for binding. This is further supported by competition binding assays that show that GTP strongly inhibits DNA binding while dATP does so to a lesser extent. Furthermore, mutation of R451, which forms cation-pi interactions with the guanine base in RS1, abolishes ssDNA binding. Taken together these data lead us to conclude that SAMHD1 binds ssDNA at the dimer interface primarily through interactions of dG nucleotides with the RS1 site providing specificity. The structures also suggest how SAMHD1 oxidation enhances ssDNA binding. We observe that ssDNA binding competes with regulatory nucleotides for binding at the RS1 and RS2 sites. Previous data also show that single-stranded nucleic acids bind to the interface of SAMHD1 and pre-

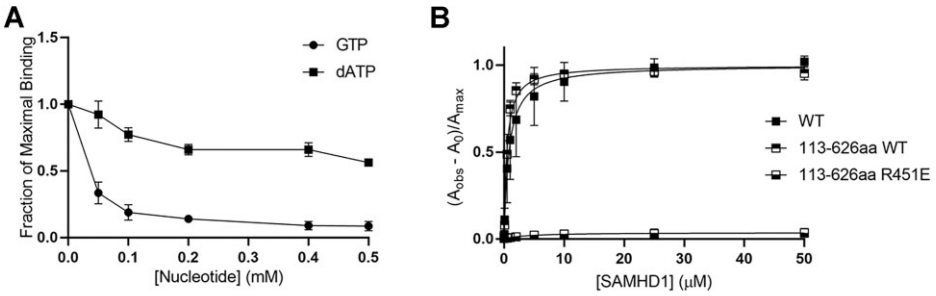

C

DNA	SAMHD1	K_d (μM)
ssDNA	$SAMH1^{WT}$	0.8 ± 0.3 μM
ssDNA	$SAMHD1^{113\text{-}626aa}$	0.5 ± 0.1 μM
ssDNA	$SAMHD1^{113\text{-}626aaR451E}$	Undetermined

Figure 4. ssDNA binds in regulatory site 1. (**A**) Analysis of oxidized SAMHD1 binding to ssDNA 30mer in the presence of activating nucleotides (GTP or dATP). The graph shows the fraction of maximal binding as a function of the nucleotide concentration. Error bars represent standard deviation. (**B**) SAMHD1 DNA binding to ssDNA under oxidizing conditions. The graph represents normalized anisotropy values relative to protein concentration. All error bars represent standard deviation. Dissociation constants (K_d) were calculated by fitting the data to the equation for one site specific binding (equation 2 in Materials and Methods). Binding of SAMHD1 WT, 113–626aa, and 113–626aa R451E to 5′ FAM labeled ssDNA 30mer. (**C**) Calculated binding affinities ±95% confidence interval for oxidized SAMHD1 WT, 113–626aa WT and 113–626aa R451E for 5′ FAM labeled ssDNA 30mers.

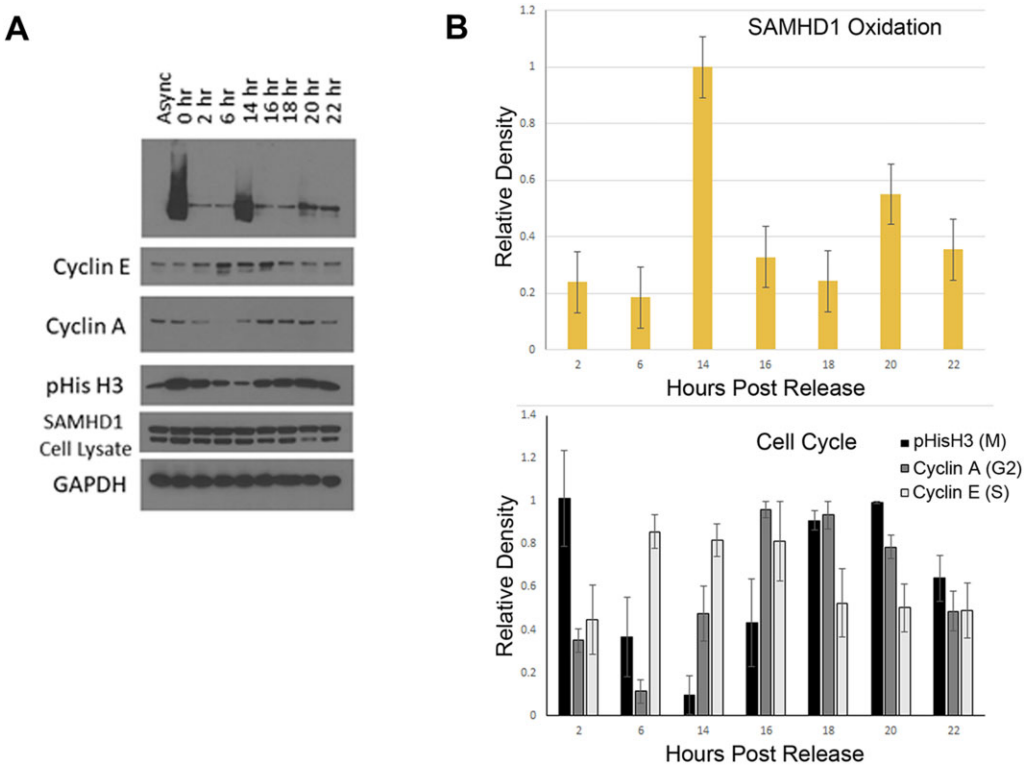

Figure 5. SAMHD1 oxidation is cell cycle-dependent. (**A**) PC3 cells were synchronized at the G_2/M transition and harvested over the course of the cell cycle. Oxidized proteins were labeled with DCP-Bio1 and captured with streptavidin beads. Labeled and captured proteins were separated by SDS-PAGE gel and transferred to nitrocellulose then probed with an anti-SAMHD1 antibody. Total cell lysate was probed for expression of SAMHD1, GAPDH, and cell cycle markers cyclin E, cyclin A, and pHis H3. (**B**) Quantitation of protein expression levels from blots shows SAMHD1 oxidation (top panel) coincides with cyclin E and cyclin A expression (S phase and G2/M transition) (bottom panel). Quantitation is from three independent experiments and error bars represent standard error of the mean.

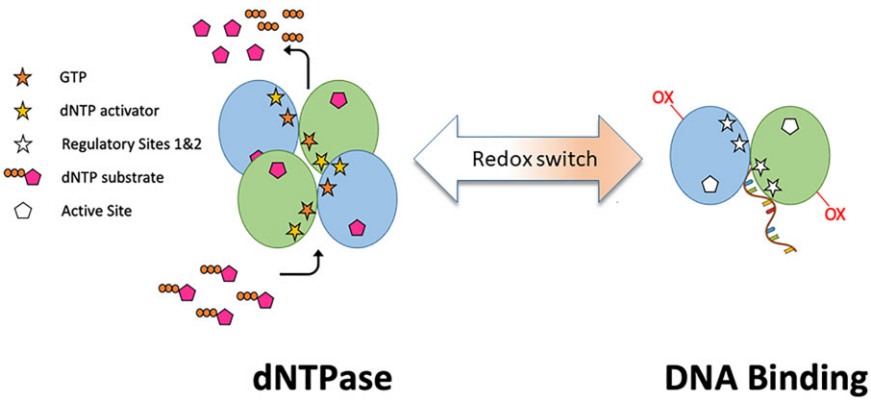

Figure 6. Model for regulation of SAMHD1 function by oxidation. Oxidation of SAMHD1 acts as a functional switch to shift SAMHD1 from dNTPase activity to DNA binding and repair.

vent formation of the tetramer (23). In the presence of both nucleic acid and regulatory nucleotides mixed occupancy SAMHD1 oligomer species are possible (27), suggesting there is a dynamic equilibrium between DNA binding, nucleotide binding and SAMHD1 oligomerization. Oxidation of SAMHD1 prevents SAMHD1 tetramerization (9) and likely pushes the equilibrium towards the dimer state and DNA binding. The current structures reveal the conformational changes that prevent the tetramer interactions from occurring when ssDNA in bound to the SAMHD1 dimer. Additionally, the specificity for ssDNA is revealed in the structure by the specific interactions with the guanine containing nucleotide within the RS1 binding site. These interactions, necessary for binding, are likely sterically hindered in dsDNA thus preventing binding.

We have previously shown that oxidation of SAMHD1 inhibits protein tetramerization and catalytic activity (9). Here the structure of the oxidized SAMHD1 protein in complex with ssDNA reveals it binds as a dimer. Interestingly, the oligomerization of other proteins has also been shown to be redox sensitive (43–47). The 2-cysteine family of peroxiredoxin (Prx) enzymes are known to form 2 oligomeric states, a decameric form of the reduced protein and a dimer form when oxidized. These enzymes belong to a large structural family that exists in bacteria to humans, and suggests that redox regulation of protein structure is a very ancient mechanism.

Recent studies have implicated SAMHD1 in repair of double-strand breaks. SAMHD1 recruits MRE11 and CtIP to double-strand breaks allowing for the initial end resection required for repair of stalled replication forks and HR (15,19). This function is independent of SAMHD1 dNTPase catalytic activity (15,19). Recent data also suggests that deacetylation of SAMHD1 by SIRT1 facilitates its binding with ssDNA at DSBs (48). In contrast, SAMHD1 catalytic activity appears necessary for efficient NHEJ to prevent long insertions occurring during repair of DSBs (21,22). In examining SAMHD1 interactions with DNA overhangs and fork structures mimicking those found at DSBs, we found two different binding modes. The interactions between SAMHD1 and the 5′ overhang or fork structures fit to a single-site binding model, whereas, the interactions between SAMHD1 and 3′ overhang and 3′ fork show cooperative binding. These constructs represent the pre- and post-resection states of DSBs during HR, and may reflect an asymmetry in the processing of the two types of DNA ends.

We previously showed that oxidation of SAMHD1 could occur in response to growth factor stimulation (9,11), but have now demonstrated that it also happens in a cell cycle-dependent fashion. Previously we showed that oxidized SAMHD1 accumulated in the cytoplasm but rapidly relocated to the nucleus, and that SAMHD1 restricted to the nucleus was not oxidized (9,11). Similarly, others have demonstrated that SAMHD1 is a nucleocytoplasmic shuttling protein (49). Thus the available data suggest that SAMHD1 translocates to the cytoplasm for oxidation, but then relocalizes to the nucleus. The fact that oxidation of SAMHD1 inhibits catalytic activity and increases DNA binding suggests that oxidation functions as a switch to promote the SAMHD1 DNA repair function. Our observation that SAMHD1 is oxidized during S-phase and the G2/M transition could be a mechanism to shift SAMHD1 to its DNA repair role, as HR occurs during these phases of the cell cycle. Additionally SAMHD1 oxidation during these phases would inhibit dNTPase function and allow dNTPs to rise to the levels necessary for genome replication. As a regulator of both dNTP levels and DNA repair mechanisms, SAMHD1 performs dual roles that are critical for replication fidelity. The identification of protein oxidation as a potential 'function-switch' between these roles highlights the importance of post-translational modifications in directing SAMHD1 function.

DATA AVAILABILITY

The structures of the SAMHD1-ssDNA complexes have been deposited in the Protein Data Bank with accession numbers 8D94 and 8D9J.

SUPPLEMENTARY DATA

Supplementary Data are available at NAR Online.

ACKNOWLEDGEMENTS

Author contributions: Conceptualization: T.L.S., S.B, L.C.R., T.H.; Methodology: T.L.S., S.B., L.C.R., O.J.Z., T.H.; Writing-original draft: T.L.S., T.H.; Writing-review and editing: T.L.S., S.B., L.C.R., T.H.

FUNDING

National Institute of General Medical Sciences [RO1 GM108827A]; Comprehensive Cancer Center of Wake Forest University National Cancer Institute (Center Support Grant [P30CA012197-47]; NIH Predoctoral Fellowships [T32-GM095440 to S.B., T32-AI007401 to T.S.]. Funding for open access charge: Departmental funds.
Conflict of interest statement. None declared.

REFERENCES

1. Powell,R.D., Holland,P.J., Hollis,T. and Perrino,F.W. (2011) Aicardi-Goutieres syndrome gene and HIV-1 restriction factor SAMHD1 is a dGTP-regulated deoxynucleotide triphosphohydrolase. *J. Biol. Chem.*, **286**, 43596–43600.
2. Goldstone,D.C., Ennis-Adeniran,V., Hedden,J.J., Groom,H.C.T., Rice,G.I., Christodoulou,E., Walker,P.A., Kelly,G., Haire,L.F., Yap,M.W. *et al.* (2011) HIV-1 restriction factor SAMHD1 is a deoxynucleoside triphosphate triphosphohydrolase. *Nature*, **480**, 379–382.
3. Mauney,C.H. and Hollis,T. (2018) SAMHD1: recurring roles in cell cycle, viral restriction, cancer, and innate immunity. *Autoimmunity*, **51**, 96–110.
4. Ji,X., Wu,Y., Yan,J., Mehrens,J., Yang,H., DeLucia,M., Hao,C., Gronenborn,A.M., Skowronski,J., Ahn,J. *et al.* (2013) Mechanism of allosteric activation of SAMHD1 by dGTP. *Nat. Struct. Mol. Biol.*, **20**, 1304–1309.
5. Yan,J., Kaur,S., DeLucia,M., Hao,C., Mehrens,J., Wang,C., Golczak,M., Palczewski,K., Gronenborn,A.M., Ahn,J. *et al.* (2013) Tetramerization of SAMHD1 is required for biological activity and inhibition of HIV infection. *J. Biol. Chem.*, **288**, 10406–10417.
6. Ji,X., Tang,C., Zhao,Q., Wang,W. and Xiong,Y. (2014) Structural basis of cellular dNTP regulation by SAMHD1. *Proc. Natl. Acad. Sci. U.S.A.*, **111**, E4305–E4314.
7. Zhu,C., Gao,W., Zhao,K., Qin,X., Zhang,Y., Peng,X., Zhang,L., Dong,Y., Zhang,W., Li,P. *et al.* (2013) Structural insight into dGTP-dependent activation of tetrameric SAMHD1 deoxynucleoside triphosphate triphosphohydrolase. *Nat. Commun.*, **4**, 2722.
8. Zhu,C., Wei,W., Peng,X., Dong,Y., Gong,Y. and Yu,X.F. (2015) The mechanism of substrate-controlled allosteric regulation of SAMHD1 activated by GTP. *Acta Crystallogr., Sect. D*, **71**, 516–524.
9. Mauney,C.H., Rogers,L.C., Harris,R.S., Daniel,L.W., Devarie-Baez,N.O., Wu,H., Furdui,C.M., Poole,L.B., Perrino,F.W. and Hollis,T. (2017) The SAMHD1 dNTP triphosphohydrolase is controlled by a redox switch. *Antioxid. Redox. Signal.*, **27**, 1317–1331.
10. Wang,Z., Bhattacharya,A., White,T., Buffone,C., McCabe,A., Nguyen,L.A., Shepard,C.N., Pardo,S., Kim,B., Weintraub,S.T. *et al.* (2018) Functionality of redox-active cysteines is required for restriction of retroviral replication by SAMHD1. *Cell Rep.*, **24**, 815–823.
11. Batalis,S., Rogers,L.A.C., Hemphill,W.O., Mauney,C.H., Ornelles,D.A. and Hollis,T. (2021) SAMHD1 phosphorylation at T592 regulates cellular localization and S-phase progression. *Front. Mol. Biosci.*, **8**,724870.
12. Patra,K.K., Bhattacharya,A. and Bhattacharya,S. (2019) Molecular dynamics investigation of a redox switch in the anti-HIV protein SAMHD1. *Proteins Struct. Funct. Bioinforma.*, **87**, 748–759.
13. Clifford,R., Louis,T., Robbe,P., Ackroyd,S., Burns,A., Timbs,A.T., Wright Colopy,G., Dreau,H., Sigaux,F., Judde,J.G. *et al.* (2014) SAMHD1 is mutated recurrently in chronic lymphocytic leukemia and is involved in response to DNA damage. *Blood*, **123**, 1021–1031.
14. Cabello-Lobato,M.J., Wang,S. and Schmidt,C.K. (2017) SAMHD1 Sheds moonlight on DNA double-strand break repair. *Trends Genet.*, **33**, 895–897.
15. Daddacha,W., Koyen,A.E., Bastien,A.J., Head,P.E., Dhere,V.R., Nabeta,G.N., Connolly,E.C., Werner,E., Madden,M.Z., Daly,M.B. *et al.* (2017) SAMHD1 Promotes DNA end resection to facilitate DNA repair by homologous recombination. *Cell Rep.*, **20**, 1921–1935.
16. Medeiros,A.C., Soares,C.S., Coelho,P.O., Vieira,N.A., Baqui,M.M.A., Teixeira,F.R. and Gomes,M.D. (2018) DNA damage response signaling does not trigger redistribution of SAMHD1 to nuclear foci. *Biochem. Biophys. Res. Commun.*, **499**, 790–796.
17. Thientosapol,E.S., Bosnjak,D., Durack,T., Stevanovski,I., Van Geldermalsen,M., Holst,J., Jahan,Z., Shepard,C., Weninger,W., Kim,B. *et al.* (2018) SAMHD1 enhances immunoglobulin hypermutation by promoting transversion mutation. *Proc. Natl. Acad. Sci. U.S.A.*, **115**, 4921–4926.
18. Majerska,J., Feretzaki,M., Glousker,G. and Lingner,J. (2018) Transformation-induced stress at telomeres is counteracted through changes in the telomeric proteome including SAMHD1. *Life Sci. Alliance*, **1**, e201800121.
19. Coquel,F., Silva,M.J., Técher,H., Zadorozhny,K., Sharma,S., Nieminuszczy,J., Mettling,C., Dardillac,E., Barthe,A., Schmitz,A.L. *et al.* (2018) SAMHD1 acts at stalled replication forks to prevent interferon induction. *Nature*, **557**, 57–61.
20. Maharana,S., Kretschmer,S., Hunger,S., Yan,X., Kuster,D., Traikov,S., Zillinger,T., Gentzel,M., Elangovan,S., Dasgupta,P. *et al.* (2022) SAMHD1 controls innate immunity by regulating condensation of immunogenic self RNA. *Mol. Cell*, **82**, 3712–3728.
21. Akimova,E., Gassner,F.J., Schubert,M., Rebhandl,S., Arzt,C., Rauscher,S., Tober,V., Zaborsky,N., Greil,R. and Geisberger,R. (2021) SAMHD1 restrains aberrant nucleotide insertions at repair junctions generated by DNA end joining. *Nucleic Acids Res.*, **49**, 2598–2608.
22. Husain,A., Xu,J., Fujii,H., Nakata,M., Kobayashi,M., Wang,J., Rehwinkel,J., Honjo,T. and Begum,N.A. (2020) SAMHD 1-mediated dNTP degradation is required for efficient DNA repair during antibody class switch recombination. *EMBO J.*, **39**, e102931.
23. Seamon,K.J., Bumpus,N.N. and Stivers,J.T. (2016) Single-stranded nucleic acids bind to the tetramer interface of SAMHD1 and prevent formation of the catalytic homotetramer. *Biochemistry*, **55**, 6087–6099.
24. Seamon,K.J., Sun,Z., Shlyakhtenko,L.S., Lyubchenko,Y.L. and Stivers,J.T. (2015) SAMHD1 is a single-stranded nucleic acid binding protein with no active site-associated nuclease activity. *Nucleic Acids Res.*, **43**, 6486–6499.
25. Goncalves,A., Karayel,E., Rice,G.I., Bennett,K.L., Crow,Y.J., Superti-Furga,G. and Bürckstümmer,T. (2012) SAMHD1 is a nucleic-acid binding protein that is mislocalized due to aicardi-goutières syndrome-associated mutations. *Hum. Mutat.*, **33**, 1116–1122.
26. Tüngler,V., Staroske,W., Kind,B., Dobrick,M., Kretschmer,S., Schmidt,F., Krug,C., Lorenz,M., Chara,O., Schwille,P. *et al.* (2013) Single-stranded nucleic acids promote SAMHD1 complex formation. *J. Mol. Med.*, **91**, 759–770.
27. Yu,C.H., Bhattacharya,A., Persaud,M., Taylor,A.B., Wang,Z., Bulnes-Ramos,A., Xu,J., Selyutina,A., Martinez-Lopez,A., Cano,K. *et al.* (2021) Nucleic acid binding by SAMHD1 contributes to the antiretroviral activity and is enhanced by the GpsN modification. *Nat. Commun.*, **12**, 731.
28. Mauney,C.H., Perrino,F.W. and Hollis,T. (2018) Identification of inhibitors of the dNTP triphosphohydrolase SAMHD1 using a novel and direct high-throughput assay. *Biochemistry*, **57**, 6624–6636.
29. Emsley,P., Lohkamp,B., Scott,W.G. and Cowtan,K. (2010) Features and development of Coot. *Biol.*, **66**, 486–501.
30. Adams,P.D., Afonine,P.V., Bunkóczi,G., Chen,V.B., Echols,N., Headd,J.J., Hung,L.W., Jain,S., Kapral,G.J., Grosse Kunstleve,R.W. *et al.* (2011) The Phenix software for automated determination of macromolecular structures. *Methods*, **55**, 94–106.
31. Williams,C.J., Headd,J.J., Moriarty,N.W., Prisant,M.G., Videau,L.L., Deis,L.N., Verma,V., Keedy,D.A., Hintze,B.J., Chen,V.B. *et al.* (2018) MolProbity: more and better reference data for improved all-atom structure validation. *Protein Sci.*, **27**, 293–315.

32. Zhang,Y. and Skolnick,J. (2004) Scoring function for automated assessment of protein structure template quality. *Proteins*, **57**, 702–710.
33. Furdui,C.M. and Poole,L.B. (2014) Chemical approaches to detect and analyze protein sulfenic acids. *Mass Spectrom. Rev.*, **33**, 126–146.
34. Saunders,J.A., Rogers,L.C., Klomsiri,C., Poole,L.B., Larry,W. and Daniel,L.W. (2010) Reactive oxygen species mediate lysophosphatidic acid induced signaling in ovarian cancer cells. *Free Radic. Biol. Med.*, **49**, 2058–2067.
35. Koharudin,L.M.I., Wu,Y., DeLucia,M., Mehrens,J., Gronenborn,A.M. and Ahn,J. (2014) Structural basis of allosteric activation of sterile α motif and histidine-aspartate domain-containing protein 1 (SAMHD1) by nucleoside triphosphates. *J. Biol. Chem.*, **289**, 32617–32627.
36. Morris,E.R., Caswell,S.J., Kunzelmann,S., Arnold,L.H., Purkiss,A.G., Kelly,G. and Taylor,I.A. (2020) Crystal structures of SAMHD1 inhibitor complexes reveal the mechanism of water-mediated dNTP hydrolysis. *Nat. Commun.*, **11**, 3165.
37. Lim,G., Chang,Y. and Huh,W.K. (2020) Phosphoregulation of Rad51/Rad52 by CDK1 functions as a molecular switch for cell cycle–specific activation of homologous recombination. *Sci. Adv.*, **6**, eaay2669.
38. Mathiasen,D.P. and Lisby,M. (2014) Cell cycle regulation of homologous recombination in Saccharomyces cerevisiae. *FEMS Microbiol. Rev.*, **38**, 172–184.
39. Zhao,X., Wei,C., Li,J.J., Xing,P., Li,J.J., Zheng,S. and Chen,X. (2017) Cell cycle-dependent control of homologous recombination. *Acta Biochim. Biophys. Sin. (Shanghai).*, **49**, 655–668.
40. Orthwein,A., Noordermeer,S.M., Wilson,M.D., Landry,S., Enchev,R.I., Sherker,A., Munro,M., Pinder,J., Salsman,J., Dellaire,G. *et al.* (2015) A mechanism for the suppression of homologous recombination in G1 cells. *Nature*, **528**, 422–426.
41. Harper,J.V. (2004) Synchronization of cell populations in G1/S and G2/M phases of the cell cycle. In *Methods Mol. Biol.*, **296**, 157–166.
42. Surani,A.A., Colombo,S.L., Barlow,G., Foulds,G.A. and Montiel-Duarte,C. (2021) Optimizing cell synchronization using nocodazole or double thymidine block. *Methods Mol. Biol.*, **2329**, 111–121.
43. Forshaw,T.E., Reisz,J.A., Nelson,K.J., Gumpena,R., Lawson,J.R., Jönsson,T.J., Wu,H., Clodfelter,J.E., Johnson,L.C., Furdui,C.M. *et al.* (2021) Specificity of human sulfiredoxin for reductant and peroxiredoxin oligomeric state. *Antioxidants*, **10**, 946.
44. Nelson,K.J., Messier,T., Milczarek,S., Saaman,A., Beuschel,S., Gandhi,U., Heintz,N., Smalley,T.L., Lowther,W.T. and Cunniff,B. (2021) Unique cellular and biochemical features of human mitochondrial peroxiredoxin 3 establish the molecular basis for its specific reaction with thiostrepton. *Antioxidants*, **10**, 150.
45. Wood,Z.A., Poole,L.B., Hantgan,R.R. and Karplus,P.A. (2002) Dimers to doughnuts: redox-sensitive oligomerization of 2-cysteine peroxiredoxins. *Biochemistry*, **41**, 5493–5504.
46. Klomsiri,C., Rogers,L.C., Soito,L., McCauley,A.K., King,S.B., Nelson,K.J., Poole,L.B. and Daniel,L.W. (2014) Endosomal H2O2 production leads to localized cysteine sulfenic acid formation on proteins during lysophosphatidic acid-mediated cell signaling. *Free Radic. Biol. Med.*, **71**, 49–60.
47. Hall,A., Karplus,P.A. and Poole,L.B. (2009) Typical 2-cys peroxiredoxins - structures, mechanisms and functions. *FEBS J.*, **276**, 2469–2477.
48. Kapoor-Vazirani,P., Rath,S.K., Liu,X., Shu,Z., Bowen,N.E., Chen,Y., Haji-Seyed-Javadi,R., Daddacha,W., Minten,E.V., Danelia,D. *et al.* (2022) SAMHD1 deacetylation by SIRT1 promotes DNA end resection by facilitating DNA binding at double-strand breaks. *Nat. Commun.*, **13**, 6707.
49. Du,J., Peng,Y., Wang,S., Hou,J., Wang,Y., Sun,T. and Zhao,K. (2019) Nucleocytoplasmic shuttling of SAMHD1 is important for LINE-1 suppression. *Biochem. Biophys. Res. Commun.*, **510**, 551–557.

© The Author(s) 2023. Published by Oxford University Press on behalf of Nucleic Acids Research.
This is an Open Access article distributed under the terms of the Creative Commons Attribution-NonCommercial License (http://creativecommons.org/licenses/by-nc/4.0/), which permits non-commercial re-use, distribution, and reproduction in any medium, provided the original work is properly cited. For commercial re-use, please contact journals.permissions@oup.com